3-D Scanning of Nonopaque Objects by Means of Imaging Emitted Structured Infrared Patterns

Fabrice Mériaudeau, L. Alonso Sánchez Secades, Gonen Eren, A. Erçil, Fred Truchetet, Olivier Aubreton, and David Fofi

***Abstract*—Three-dimensional surface acquisition is a subject that has been studied to a large extent; a significant number of techniques for acquiring shapes have been proposed, and a wide range of commercial solutions is available. Nevertheless, today's systems still have difficulties when digitizing objects that are transparent or semitransparent in the visible range. In this paper, some of the issues of traditional scanning systems are addressed by considering the radiative properties of materials. As a result, an infrared laser light-based scanner is presented for successfully acquiring the shape of complex surfaces by analyzing heat patterns that are emitted by the object.**

***Index Terms*—Laser scanner, nonopaque objects, shape-from-heating, three-dimensional shape acquisition.**

I. Introduction

RECENTLY, techniques for 3-D reconstruction of objects through observation have been extensively investigated. Such 3-D digitization techniques have a wide range of applications from virtual medical applications to 3-D object recognition. Geometry is one of the most important aspects of 3-D reconstruction since one can measure the shape of an object and compare it to its computer-aided design model to calculate its error map from its original ground truth. The computer vision community has extensively developed techniques to determine the shape of objects [1], [2]. Laser-light-based scanning systems are probably the most commonly used solution for acquiring the 3-D shape of objects [15]; however, for nonopaque materials, there is no applicable solution available yet. To recover the 3-D shape, powder is usually used to change the surfaces to diffuse surfaces. This is troublesome, and the thickness of powder influences the accuracy of 3-D measurement. Recently, Saito *et al.* [3] and Myasaki *et al.* [4], [5] have developed a technique relying on the "shape from polarization," which was, later on, applied to metallic specular surfaces [27]. Even so, recent technology enables high-speed polarization imaging [13]; the experimental procedure of this technique is too complicated for outside laboratory applications. Recent works based on polarization coupled with inverse ray tracing [6] led to promising results, which cope with some of the cons of the previous methods by taking into account the interreflections and not suffering from the ambiguity of the incident angle. However, this technique is still based on numerous assumptions such as a known back surface shape, a known refractive index, and a homogenous lighting system that cannot be guaranteed for any object shape. Other methods that estimate the 3-D shape of transparent objects without using polarization have been proposed. Hata *et al.* [7] and Yamazaki *et al.* [18] estimated the surface shape of transparent objects by analyzing the deformation of the light that is projected onto the transparent objects. Morris and Kutulakos [42] proposed a method based on scatter-trace photography that provides good results for complex objects with an inhomogeneous interior. Ohara *et al.* [8] estimated the depth of the edge of a transparent object by using the shape from focus. Ben-Ezra and Nayar [9] used the structure from motion to estimate the parameterized surface shape of transparent objects. These methods, however, do not estimate the arbitrary shapes of transparent objects. Trifonov *et al.* [10] have recently estimated the shape of a transparent object through visible tomography. However, their technique requires immersing in a liquid the object to be digitized and assumes perfect index matching (to avoid spurious interreflections) between the fluid and the object. Hullin *et al.* [41] have developed a similar technique by immersing the object to be digitized in fluorescent liquid. Other techniques such as conoscopic holography, dynamic lighting, reflection models, or other model minimization-based techniques have been proposed; however, a fast and accurate noncontact acquisition technique for non-Lambertian surfaces has not yet been developed [21]–[26], [28].

This paper presents a new approach for addressing some of the issues of visible light laser scanners (Fig. 1) by considering the radiative properties of materials. An example analysis for soda-lime glass objects is presented, and a prototype *IR* laser scanner is developed for demonstrative purposes.

Similar techniques based on an *IR* sensor to infer 3-D information have recently been developed: Pelletier and Maldague [19] were among the pioneers to work on this idea. Their technique ("shape from heating") requires a presegmentation of the image to isolate linear patches and nonlinear patches, which are, afterward, used to lead to "extraction of relative depth" and "extraction of surface orientation." The technique is restricted to simple shapes such as cylinders, and accurate measurements for more complex objects have not yet been achieved. An

Manuscript received July 15, 2009; revised November 23, 2009; accepted December 23, 2009. Date of current version October 13, 2010. The Associate Editor coordinating the review process for this paper was Dr. George Xiao.

F. Mériaudeau, L. Alonso Sánchez Secades, F. Truchetet, O. Aubreton, and D. Fofi are with the Laboratory Le2i, Unite Mixte de Recherche, Centre National de la Recherche Scientifique 5158, University de Bourgogne, 71200 Le Creusot, France (e-mail: fmeriau@u-bourgogne.fr).

G. Eren is with the Sabanci University, 34956 Istanbul, Turkey, with the Laboratory Le2i, UMR CNRS 5158, University de Bourgogne, 71200 Le Creusot, France, and also with the Department of Computer Engineering, Galatasaray University, 34357 Istanbul, Turkey.

A. Erçil is with the Sabanci University, 34956 Istanbul, Turkey.

Color versions of one or more of the figures in this paper are available online at http://ieeexplore.ieee.org.

Digital Object Identifier 10.1109/TIM.2010.2046694

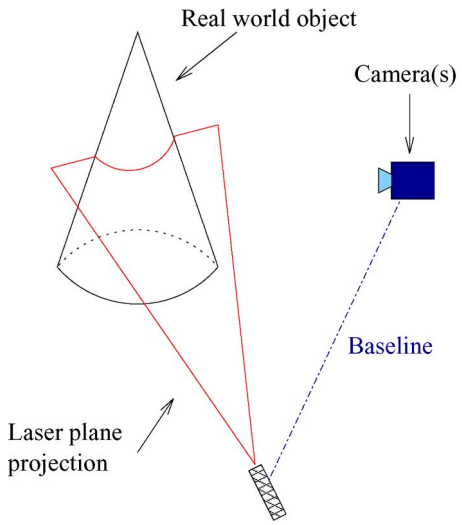

Fig. 1. Laser-triangulation-based scanner; the pattern deformation is analyzed to determine the depth.

extension of this technique, called the "shape from amplitude," has recently been proposed [20]. The technique uses amplitude images that are obtained in pulse phase thermography. Ming *et al.* [11], [12] calibrated an *IR* camera that acquires a sequence of 2-D thermographic images and then reconstructed the 3-D temperature distribution from the captured 2-D thermal images by the Octree carving technique. This technique is based on imaging the heat released by a surface that is being mechanically processed and is, by its principle, close to our system; however, the 3-D reconstruction principle based on the shape from silhouette is totally different from our technique. Sadjadi [14], [16] and Prakash *et al.* [17] proposed a passive stereoscopic system. Both techniques suffer from the lack of texture on *IR* images leading to a sparse 3-D representation. To cope with this lack of information, our system relies on an *IR* pattern that is being simply projected onto the object [39], and the heat released by the object (which has been heated by the *IR* radiation) is then imaged by a spatially calibrated *IR* sensor; the technique relies, therefore, on the observation of the emitted pattern.

The rest of this paper is organized as follows: The first part presents the background that is related to the radiative properties of a material. The second part deals with our model of laser heating, and some simulations are presented. The third part is related to our 3-D laser scanning method and explains our calibration technique based on the complete quadrangle and the cross ratio. The last part is dedicated to some results that show the efficiency of our method. This paper ends with a short conclusion that presents our contribution, as well as some insights for future work.

II. Radiative Properties of Materials

When the literature refers to nonopaque materials or non-Lambertian surfaces, it usually means that the material properties allow visible light to pass through or that the light is reflected in a particular way (Fig. 2). Nonetheless, the electromagnetic radiation outside the visible spectrum also interacts with matter in a manner that could be described as a combination of transmission, reflection, and absorption of energy. For example, flesh is transparent to X-rays, while bone is not, making X-ray imaging useful for medicine.

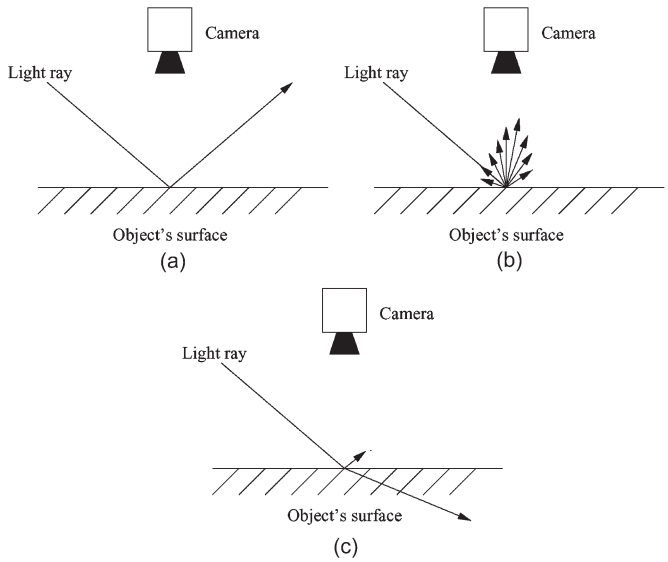

Fig. 2. Behavior of light on different surfaces. (a) Specular surface. (b) Diffuse surface. (c) Transparent surface.

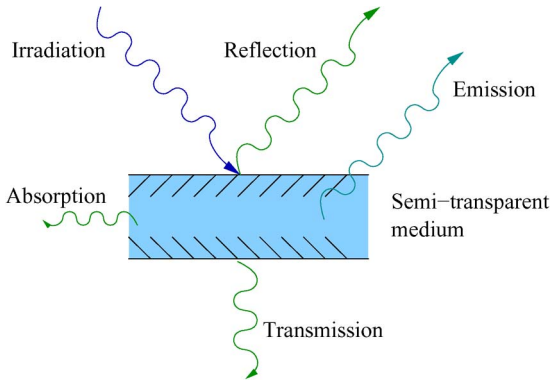

Fig. 3. Response of a semitransparent medium to electromagnetic radiation.

As in the case of X-rays, by studying the radiative properties of materials, it is possible to adapt different shape acquisition techniques to work with surfaces that are normally impossible to scan using visible light sources. A special case using *IR* imaging was developed.

Fig. 3 illustrates three possible responses of a semitransparent medium to irradiation. Without having to enter into details, from the heat transfer theory, it is possible to establish a radiation balance, where the irradiation equals the sum of the reflection, absorption, and transmission terms, i.e.,

$$G_\lambda = G_{\lambda,\mathrm{refl}} + G_{\lambda,\mathrm{abs}} + G_{\lambda,\mathrm{trans}}. \tag{1}$$

To quantify the amount of irradiation being absorbed, reflected, and transmitted, different coefficients have been defined (i.e., α, ρ, and τ, respectively). In the most general case and assuming negligible temperature dependence, these coefficients depend on the angle of incidence θ and on the radiation wavelength λ. Then, for a particular medium, the following balance can be derived:

$$\alpha_{\theta,\lambda} + \rho_{\theta,\lambda} + \tau_{\theta,\lambda} = 1. \tag{2}$$

TABLE I
SUMMARY OF SOME THERMAL PROPERTIES OF SODA-LIME GLASS AND AIR

Property name	Value	Units
Thermal conductivity	$0.96, \ldots, 1.10$	$W/(mK)$
Specific heat capacity c	0.84	$kJ/(kgK)$
Density ρ	$2400, \ldots, 2800$	kg/m^3
Emissivity ϵ	$0.75, \ldots, 0.92$	–
Thermal conductivity of air (20°C)	0.03	$W/(mK)$
Glass transition temperature	over 833	K
Critical tension stress	70	MPa

Finally, Kirchoff's law equates the following spectral directional properties:

$$\alpha_{\theta,\lambda} = \epsilon_{\theta,\lambda} \tag{3}$$

where ϵ is the surface emissivity. It is only a contrast between the emission of a particular body and the ideal behavior of a black body at the same temperature.

Different materials have different absorption, reflection, and transmission coefficients, depending on the radiation wavelength λ. At wavelengths over 5 μm, glass is no longer transparent and, on the contrary, presents a behavior that is a combination of reflection and absorption [39]. In general, most materials absorb radiation with wavelengths over 5 μm, and this results into an increase in temperature. The increase in temperature can then be observed with a spatially calibrated camera to recover the 3-D coordinates of the object.

Some of the thermal properties that will be useful for studying the behavior of soda-lime glass are summarized in Table I.

III. LASER HEATING MODEL FOR SIMULATION

At the working wavelengths, most suitable imaging sensors are very sensitive to direct irradiation, and they can be damaged. For this reason, only the generated heating pattern (re-emitted by the surface) will be analyzed. To do so, when the laser beam is on, the camera field of view is obstructed by a construction material, and then the beam is obstructed when the camera sees the heat-released pattern.

To determine the optimal parameters and limitations for acquiring image sequences (i.e., heating time, cooling time, laser shape, laser power, minimum acquisition time, etc.), a model for studying the laser heating of glass is used. Furthermore, it would be possible to ensure that the operating conditions are such that the material characteristics will not be altered (i.e., burning or melting the material, creating fractures due to stress, or degrading any of the surface properties).

Many authors have studied the laser heating of glass [29]–[33]. Jiao and Wang [29], similarly to Tian and Chu [30], explored the possibility of considering the laser as a volumetric heating source and as a superficial source. As the experimental results revealed, the latter assumption suffices for our analysis.

The following additional assumptions are made.

1) Since a narrow temperature range is studied, all the thermodynamic parameters of glass are considered to be isotropic and temperature independent.
2) The temperature of the glass under the laser irradiation is lower than the transition temperature of soda-lime glass (Table I), and the tension stress is lower than the critical value of the fracture (70 MPa). Hence, the phase change and the cutting groove are not considered.
3) Heat transfer is not affected by thermal expansion. Inertia effects are negligible.
4) The laser beam is regarded as a surface-heating source [30].
5) The superficial heat irradiation is negligible in the area without laser heating.

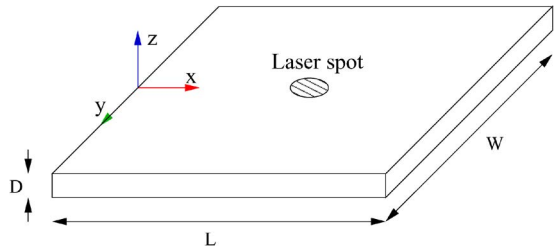

Fig. 4. Piece of glass irradiated by an *IR* laser beam.

According to the previous assumptions and with the reference system shown in Fig. 4, the following system of differential equations can be established [34]:

$$\underbrace{\rho c \frac{\partial T}{\partial t} = k \nabla^2 T}_{\text{Heat equation}} \tag{4}$$

$$\underbrace{T(0) = T_0}_{\text{Initial conditions}} \tag{5}$$

$$\underbrace{-k\frac{\partial T}{\partial z}}_{\text{Conduction}} + \underbrace{h(T - T_{\text{ext}})}_{\text{Convection}} + \underbrace{\sigma\epsilon\left(T^4 - T_{\text{ext}}^4\right)}_{\text{Radiation}} = \underbrace{\alpha I(x,y,z,t)}_{\text{Irradiation}} \tag{6}$$

at $z = 0$ and

$$\underbrace{-k\frac{\partial T}{\partial n}}_{\text{Conduction}} = \underbrace{h(T_n - T_{\text{ext}})}_{\text{Convection}}, \text{ outside the laser spot} \tag{7}$$

where k is the thermal conductivity of glass, c and ρ are the heat capacity and the material density, respectively, T_0 is the initial temperature of glass, T_{ext} is the environment temperature, T_n denotes the temperature of the area without laser heating, h is the convection heat-transfer coefficient with air, σ is the Stefan–Boltzmann constant, $I(x, y, z, t)$ is the density of the laser power, α is the absorption coefficient, and n is the direction cosine of a boundary.

The density I of the laser power can be described by a uniform distribution and an impulse function, so that for a laser with optical power P_0

$$I(x,y,z,t) = \frac{P_0}{\pi r^2}\delta(z) \; \forall \; x^2 + y^2 < r^2 \; \in \; \Re. \qquad (8)$$

Then, the solution of these equations can easily be approximated by using the finite-element method.

For the simulation, the following parameters were used.

- The glass material parameters are obtained from Table I.
- The heat flux for the laser spot boundary condition (boundary 1) is set according to (8), so that it corresponds to laser optical power of 400 mW, and the beam diameter is 2.4 mm.
- A convection heat transfer coefficient of 10 $\mathrm{W}/(\mathrm{m}^2 \cdot \mathrm{K})$ is assumed.
- The external temperature is set to 300 K.
- Only idealized radiation is considered using an emissivity value of $\epsilon = 0.92$.
- A time step of 20 ms, which corresponds to the minimum acquisition period of the *IR* camera, and a total simulation time of 7 s are set.

Fig. 5 presents some of the results that are obtained using our model.

IV. Three-Dimensional Laser Scanning

As in the case of a standard laser scanner, a laser peak detection method is required for determining the image pixels where the laser pattern is located. Since the object to be scanned is initially at temperature T0, after projecting a laser plane, the temperature along the intersection with the object's surface will rise. To segment the interest region, it is only necessary to threshold the image at a given temperature, which is selected by analyzing the image histogram. According to the energy conservation principle, under the absence of any other heat sources, it is guaranteed that the temperature gradient at the laser intersection will be maximum. In our configuration, some background reflections were removed by a region-growing approach and selection of the longest region (due to the laser line; Fig. 6). Subsequently, the laser peak is found by computing the zero crossing of the segmented temperature gradient along the x-direction (Fig. 7; i.e., the first derivative along the segmented image rows) [35].

Finally, a calibration algorithm based on the concept of the complete quadrangle was used to obtain a transformation that relates the extracted image pixels with the real 3-D world coordinates. Indeed, some other calibration techniques perform an initial calibration for obtaining the camera's intrinsic parameters and the location of a reference plane, and then perform a second calibration step for the laser plane (see [36]). This is not suitable since a custom *IR* calibration rig has to be designed, and the imaging parameters have to be set up for the first camera calibration. Briefly, this technique is based on elementary concepts from projective geometry [38], [40] that will be summarized hereafter. Let us first introduce the cross ratio of a pencil of four lines, defined by the four points of the intersection of a fourth line, not penetrating the pencil.

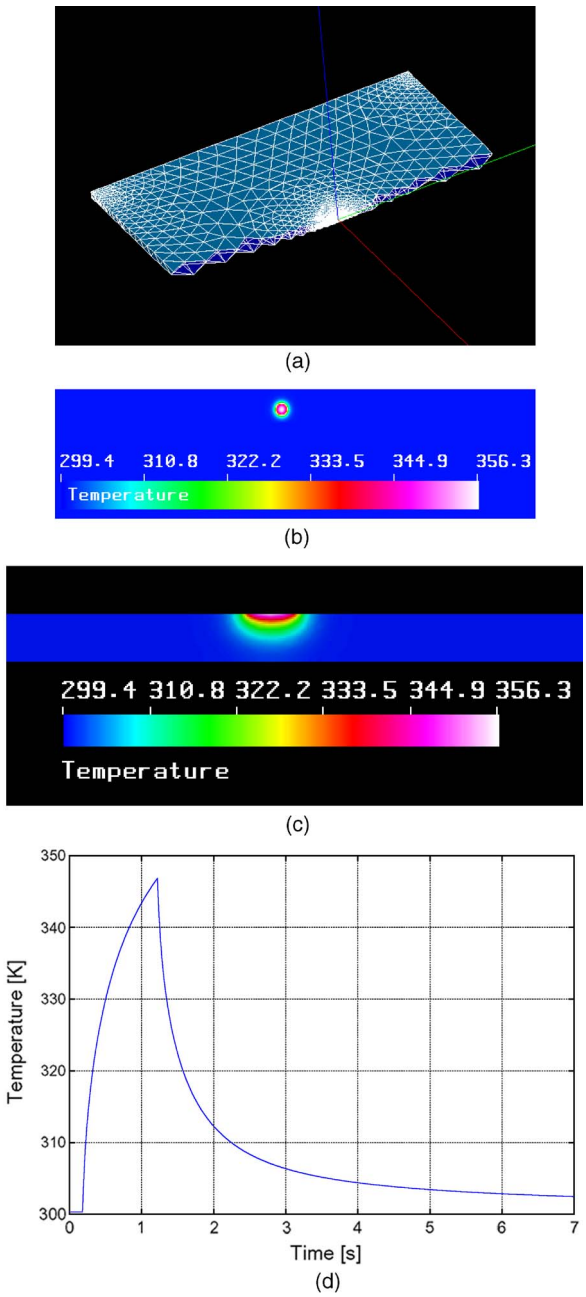

Fig. 5. Three-dimensional mesh generation for finite element analysis (FEA). (a) Three-dimensional mesh of nodes. (b) Front view of the simulation results at $t = 1.24$ s. (c) Transversal cut to visualize the volumetric heat transfer. (d) Simulated average temperature evolution at the laser spot.

The intersection points A, B, C, and D are shown in Fig. 8. Equations (9) and (10) define the cross ratio, where λ_1, λ_2, and λ_3 refer to the distances $\overline{AB}$, $\overline{AC}$, and $\overline{AD}$, respectively, and λ_1', λ_2', and λ_3' refer to the distances $\overline{A'B'}$, $\overline{A'C'}$, and $\overline{A'D'}$, respectively, i.e.,

$$Cr\{A,B;C,D\} = k = \frac{\overline{AC}.\overline{BD}}{\overline{AD}.\overline{BC}} \qquad (9)$$

$$k = \frac{\lambda_2 \cdot (\lambda_3 - \lambda_1)}{\lambda_3 \cdot (\lambda_2 - \lambda_1)} \qquad (10)$$

$$\lambda_2' = \frac{k \cdot \lambda_3' \cdot \lambda_1'}{(k-1) \cdot \lambda_3' + \lambda_1'}. \qquad (11)$$

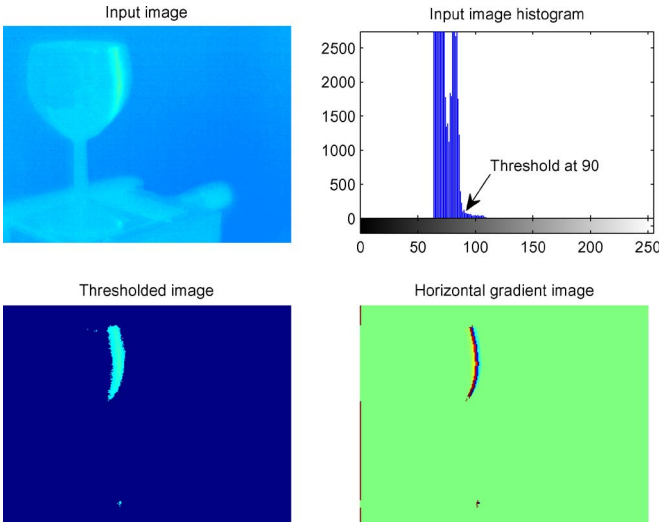

Fig. 6. Laser peak detection.

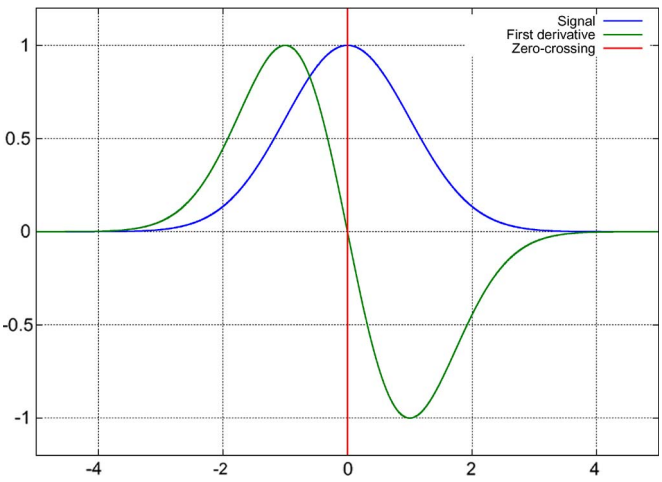

Fig. 7. Subpixel determination of the laser peak.

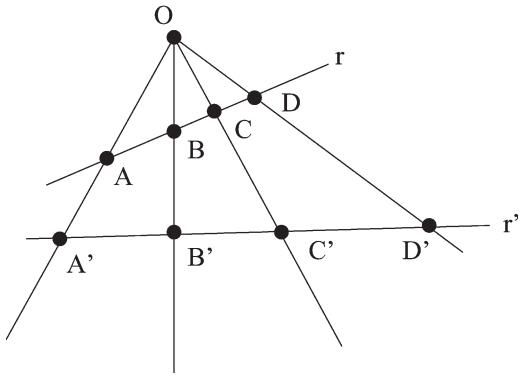

Fig. 8. Cross ratio of a pencil of lines.

It can be demonstrated that under projective transformations, the cross ratio is invariant and is useful for determining any fourth projected point from the knowledge of only three points [35].

The complete quadrangle, on the other hand, is any set of four nonaligned points, as shown in Fig. 9. It defines seven points in total, i.e., A to G, and the pencil of four lines based

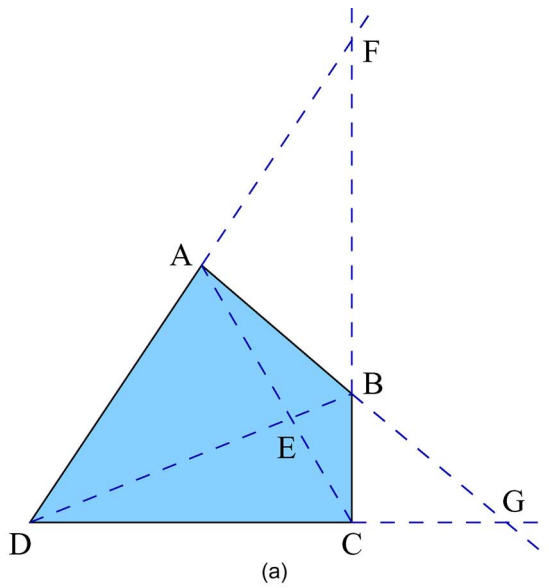

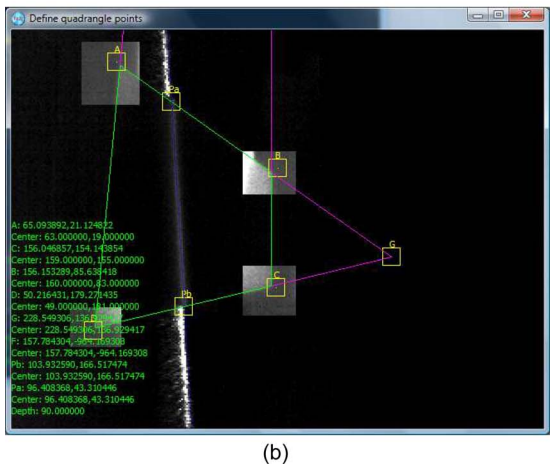

Fig. 9. Complete quadrangle principle. (a) Complete quadrangle. (b) Quadrangle made of glass for the calibration and visualization of the heat pattern released.

on the intersection of opposite sides is harmonic. For instance, $Cr\{FA, FB; FE; FG\} = -1$.

To calibrate the system, we would like to find a transformation ${}^{W}T_{L}$ between the 3-D surface points and the extracted image points (Fig. 10). This can be linearly approximated by

$$\begin{bmatrix} sX \\ sY \\ sZ \\ s \end{bmatrix} = {}^{W}T_{L\,(4\times3)} \cdot \begin{bmatrix} u \\ v \\ 1 \end{bmatrix} = \begin{bmatrix} t_{11} & t_{12} & t_{13} \\ t_{21} & t_{22} & t_{23} \\ t_{31} & t_{32} & t_{33} \\ t_{41} & t_{42} & t_{43} \end{bmatrix} \cdot \begin{bmatrix} u \\ v \\ 1 \end{bmatrix}. \tag{12}$$

Arranging and grouping the terms, a homogeneous system of three equations with 12 unknowns is obtained, and it can be solved using the total least squares technique.

Triangulation is a straightforward step since, from (12), it is evident that once ${}^{W}T_{L}$ is known, 2-D points in the image frame can be directly transformed to 3-D points in the world reference frame by a simple matrix dot product operation.

As a previous step, the 2-D image points are uniquely determined by using the previously proposed laser peak detection method.

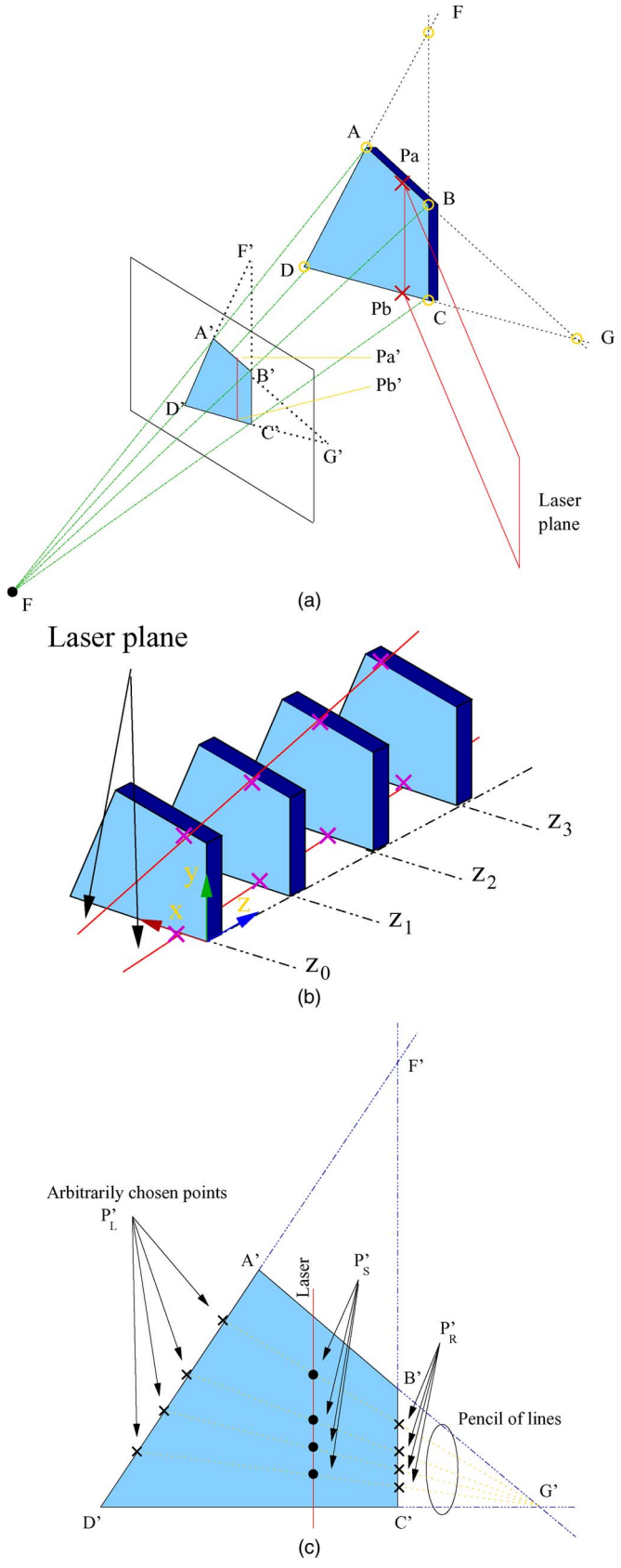

Fig. 10. Experimental calibration procedure. (a) Determination of 2-D–3-D correspondences using the complete quadrangle. (b) Positioning of the complete quadrangle at different known depths. (c) Computation of additional correspondence points.

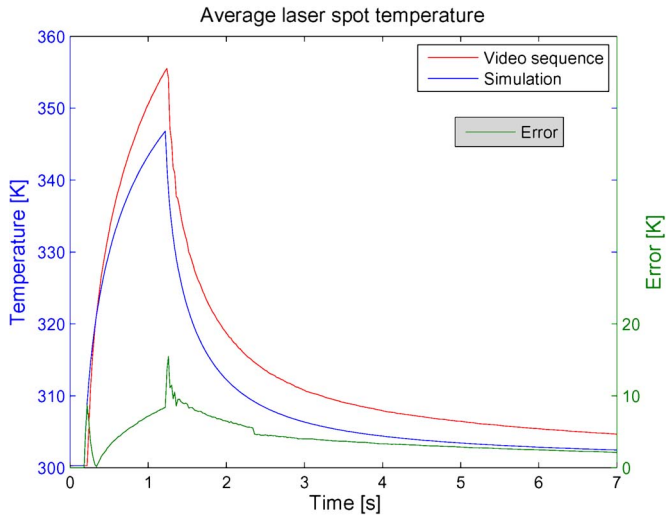

Fig. 11. Comparison of real data and simulated ones in our thermal model.

To perform the calibration step, a complete quadrangle made of glass was manufactured. Several *IR* images of this quadrangle were taken at different known depths, as illustrated in Fig. 10. To estimate the 2-D–3-D correspondences, point Pa is the first to be estimated in 3-D since we know the value of the cross ratio from the 2-D image and the value of the three other 3-D points (i.e., A, B, and G). The same situation applies for Pb and the 3-D points C, D, and G. Subsequently, additional correspondences are found by considering the points defined in Fig. 10. By selecting random points P′L in the segment A′D′, it is possible to find the corresponding 3-D points PL by computing the cross ratio value in the image plane (using points F′, A′, D′ and P′L), together with the knowledge of points F, A, and D. Then, it is only necessary to find the intersections P′r and P′s in the image plane for posteriorly using once more the cross-ratio relations to compute the most accurate correspondences for Pr and Ps. After storing the desired 2-D–3-D correspondences, one has to find transformation ${}^{W}T_{L}$ by using the total least squares technique described earlier.

V. Experimental Results

The superficial laser heating model of glass was validated by comparing the simulation results with those of a real sequence (Fig. 11). The error is mainly associated to using standard coefficient values instead of directly measuring them from the sample.

Similar simulations were performed, considering optical laser power of 400 mW, to generate a temperature difference of 1 °C during the scanning process. The experimental setup that is used for scanning is illustrated in Fig. 12.

To perform a complete 3-D reconstruction, the glass was translated in front of the experimental system by using steps of 1 mm along the x-direction. With the aim being to present the feasibility of this new technique, the 1 mm along the x-direction was chosen for convenience due to the symmetry of the inspected object, as well as to prove that heat does not have time to build up even for short displacement steps. This point will be further stressed out in a coming research study where,

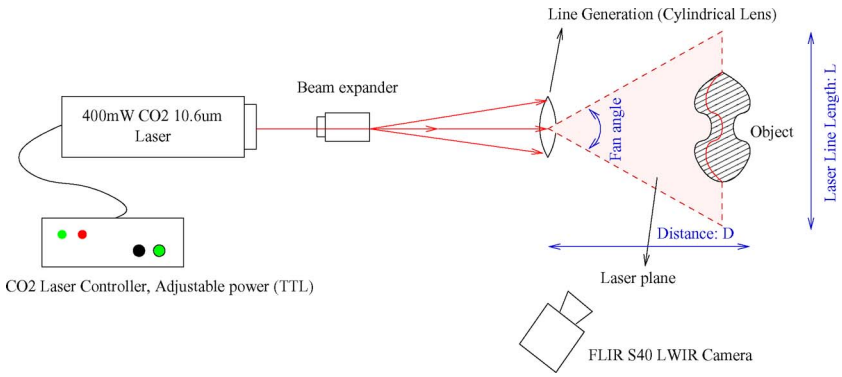

Fig. 12. Experimental setup.

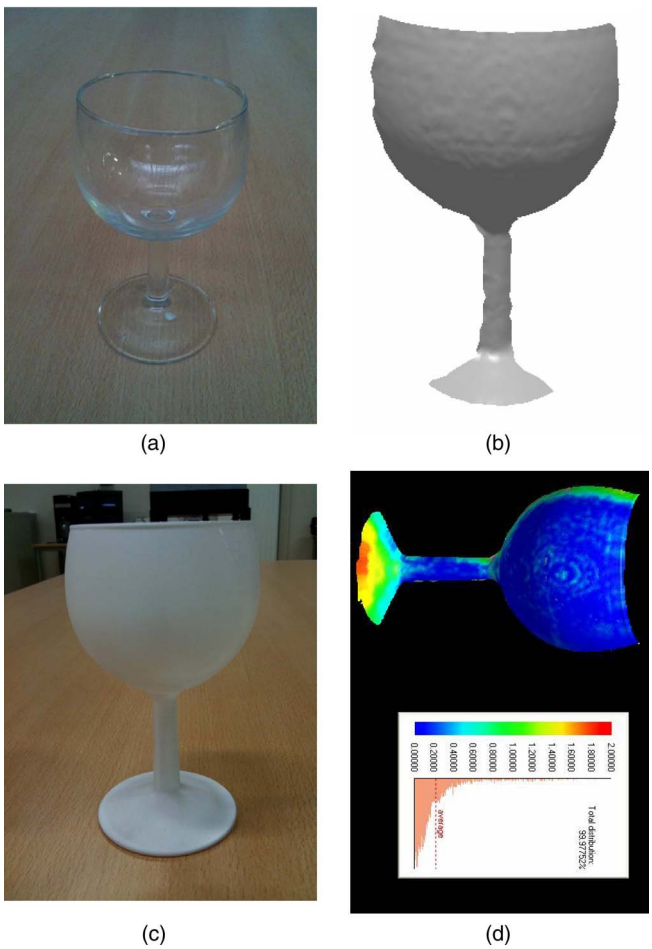

Fig. 13. Experimental results. (a) Original glass. (b) Original glass reconstruction by the shape from structured heating. (c) Glass after being coated with spray. (d) Three-dimensional reconstruction and error map, scale from 0 to 2 mm.

based on the density of the object, the temperature distribution and its evolution over time will be fully studied. The results presented below were obtained with the use of a short *IR* camera (1.5–5 μm) with a noise equivalent temperature difference of 25 mK at 25 °C and cooled by a stirling cycle. With this camera, only a small temperature difference is required to visualize the object that is heated by our 10.6-μm CO_2 laser beam, whereas more energy was required in our previous work [39].

An example of a reconstructed object and its comparison to the same object after having being coated and digitized using a commercial 3-D scanner is presented in Fig. 13.

From these measures, an error of less than 1% was found, and further experiments have to be performed to fully validate the accuracy on this new system. The larger errors on the foot of the glass are due to the commercial scanner, which is sensitive to the slope of the object due to its reflection principle, whereas our system that relies on emission is not affected.

VI. Conclusion

It has been demonstrated that it is possible to acquire the shape of nonopaque objects by studying the behavior of materials outside the visible light spectrum. Accurate point clouds of transparent glass objects have been obtained by using a prototype system that only required a single *IR* camera (a short wave is preferred, but a long wave can also be used) and *IR* laser. Well-known triangulation techniques have been successfully applied for analyzing the heating pattern deformation, providing a novel and simple method that could match the performance of other approaches such as light polarization, conoscopic holography, dynamic lightning, reflection modeling, and other model minimization methods. Finally, future work will focus on improving the mechanical setup.

Acknowledgment

The authors would like to thank the European Commission, which, through its Erasmus Mundus Program, sponsored L. Alonso Sánchez Secades during his M.Sc. in Computer Vision and Robotics (VIBOT, www.vibot.org).

References

[1] B. K. P. Horn, *Robot Vision*. Cambridge, MA: MIT Press, 1986, p. 509.
[2] D. H. Ballard and C. M. Brown, *Computer Vision*. Englewood Cliffs, NJ: Prentice Hall, 1982, p. 523.
[3] M. Saito, Y. Sato, K. Ikeuchi, and H. Kashiwagi, "Measurement of surface orientations of transparent objects by use of polarization in highlight," *J. Opt. Soc. Amer. A, Opt. Image Sci.*, vol. 16, no. 9, pp. 2286–2293, Sep. 1999.
[4] D. Miyazaki, M. Saito, Y. Sato, and K. Ikeuchi, "Determining surface orientations of transparent objects based on polarization degrees in visible and infrared wavelength," *J. Opt. Soc. Amer. A, Opt. Image Sci.*, vol. 19, no. 4, pp. 687–694, Apr. 2002.

[5] D. Miyazaki, M. Kagesawa, and K. Ikeuchi, "Transparent surface modeling from a pair of polarization images," *IEEE Trans. Pattern Anal. Mach. Intell.*, vol. 26, no. 1, pp. 73–82, Jan. 2004.
[6] D. Miyazaki and Ikeuchi, "Inverse polarization raytracing: Estimating surface shape of transparent objects," in *Proc. Int. Conf. Comput. Vis. Pattern Recog.*, San Diego, CA, Jun. 2005, vol. II, pp. 910–917.
[7] S. Hata, Y. Saitoh, S. Kumamura, and K. Kaida, "Shape extraction of transparent object using genetic algorithm," in *Proc. Int. Conf. Pattern Recog.*, 1996, pp. 684–688.
[8] K. Ohara, M. Mizukawa, K. Ohba, and K. Taki, "3D modeling of micro transparent object with integrated vision," in *Proc. IEEE Conf. Multisensor Fusion Integration Intell. Syst.*, 2003, pp. 107–112.
[9] M. Ben-Ezra and S. K. Nayar, "What does motion reveal about transparency?," in *Proc. IEEE Int. Conf. Comput. Vis.*, 2003, pp. 1025–1032.
[10] B. Trifonov, D. Bradley, and W. Heidrich, "Tomographic reconstruction of transparent objects," in *Proc. Eurographics Symp. Rendering*, T. Akenine-Möller and W. Heidrich, Ed.s, 2006, pp. 51–60.
[11] Y. Ming, H. Ng, and R. Du, "Acquisition of 3D surface temperature distribution of a car body," in *Proc. IEEE Int. Conf. Inf. Acquisition*, Hong Kong, Jun. 27–Jul. 3 2005.
[12] Y. Ming, H. Ng, M. Yu, Y. Huang, and R. Du, "Diagnosis of sheet metal stamping processes based on 3-D thermal energy distribution," *IEEE Trans. Autom. Sci. Eng.*, vol. 4, no. 1, pp. 22–31, Jan. 2007.
[13] L. Bigué and N. Cheney, "High-speed portable polarimeter using a ferroelectric liquid crystal modulator," in *Proc. SPIE*, J. A. Shaw and J. Scott Tyo, Ed.s, 2007, vol. 6682, p. 668 205.
[14] F. A. Sadjadi, "Passive 3D imaging using polarimetric diversity," *Opt. Lett.*, vol. 32, no. 3, pp. 229–231, Feb. 2007.
[15] J. Salvi, C. Matabosch, D. Fofi, and J. Forest, "A review of recent range image registration methods with accuracy evaluation," *Image Vis. Comput.*, vol. 25, no. 5, pp. 578–596, May 2007.
[16] F. A. Sadjadi, "Extraction of surface normal and index of refraction using a pair of passive infrared polarimetric sensors," in *Proc. IEEE Int. Workshop Object Tracking Classification Beyond Visible Spectr.*, Minneapolis, MN, Jun. 2007, pp. 1–5.
[17] S. Prakash, P. Y. Lee, and T. Caelli, "3D mapping of surface temperature using thermal stereo," in *Proc. IEEE ICARCV*, 2006, pp. 1–4.
[18] M. Yamazaki, S. Iwata, and G. Xu, "Dense 3D reconstruction of specular and transparent objects using stereo cameras and phase-shift method," in *Proc. ACCV*, vol. 4844, *LNCS*, Y. Yagi, S. B. Kang, I.-S. Kweon, and H. Zha, Ed.s, 2007, pp. 570–579.
[19] J. F. Pelletier and X. Maldague, "Shape from heating: A two-dimensional approach for shape extraction in infrared images," *Opt. Eng.*, vol. 36, no. 2, pp. 371–375, Feb. 1997.
[20] C. Liu, L. Czuban, P. Bison, E. Grinzato, S. Marinetti, and X. Maldague, "Complex-surfaced objects: Effects on phase and amplitude images in pulsed phase thermography," in *Proc. 12th A-PCNDT*, Auckland, New Zealand, Nov. 5–10, 2006. [Online]. Available: http: //www.ndt.net/article/apcndt2006/papers/42.pdf
[21] M. Goesele, H. P. A. Lensch, J. Lang, C. Fuchs, and H.-P. Seidel, "DISCO: Acquisition of translucent objects," *ACM Trans. Graph.*, vol. 23, no. 3, pp. 835–844, Aug. 2004.
[22] W. Matusik, H. Pfister, R. Ziegler, A. Ngan, and L. McMillan, "Acquisition and rendering of transparent and refractive objects," in *Proc. EWR*, 2002, pp. 267–278.
[23] K. Kutulakos and E. Steger, "A theory of refractive and specular 3D shape by light-path triangulation," *Int. J. Comput. Vis.*, vol. 76, no. 1, pp. 13–29, Jan. 2008.
[24] T. Bonfort, P. Sturm, and P. Gargallo, "General specular surface triangulation," in *Proc. ACCV*, 2006, pp. 872–881.
[25] M. Fanany, I. Kumazawa, and K. Kobayashi, "A neural network scheme for transparent surface modelling," in *Proc. GRAPHITE*, 2005, pp. 433–437.
[26] S. Hasinoff and K. Kutulakos, "Photo-consistent reconstruction of semi-transparent scenes by density-sheet decomposition," *IEEE Trans. Pattern Anal. Mach. Intell.*, vol. 29, no. 5, pp. 870–885, May 2007.
[27] O. Morel, C. Stolz, F. Meriaudeau, and P. Gorria, "Active lighting applied to three-dimensional reconstruction of specular metallic surfaces by polarization imaging," *Appl. Opt.*, vol. 45, no. 17, pp. 4062–4068, Jun. 2006.
[28] G. Y. Sirat, F. Paz, G. Agronik, and K. Wilner, "Conoscopic holography," *Proc. SPIE*, vol. 5972, p. 597 202, 2005.
[29] J. Jiao and X. Wang, "A numerical simulation of machining glass by dual CO2 laser beams," *Opt. Laser Technol.*, vol. 40, no. 2, pp. 297–301, Mar. 2008.
[30] W. Tian and W. Chiu, "Temperature prediction for CO2 laser heating of moving glass rods," *Opt. Laser Technol.*, vol. 36, no. 2, pp. 131–137, Mar. 2004.
[31] J. Li, L. Li, and F. H. Stott, "Comparison of volumetric and surface heating sources in the modeling of laser melting of ceramic materials," *Int. J. Heat Mass Transf.*, vol. 47, no. 6/7, pp. 1159–1174, Mar. 2004.
[32] R. Ciegis and S. Norvaisas, "Mathematical modeling of laser heating of metal," *Litovskii Matematicheskii Sbornik*, vol. 31, no. 4, pp. 687–699, Oct.–Dec. 1991.
[33] J. Lewis, "Laser heating of an optical fiber," *Appl. Opt.*, vol. 15, no. 5, pp. 1304–1306, May 1976.
[34] J. Lienhard, IV and J. Lienhard, V, *A Heat Transfer Textbook*. Cambridge, MA: Phlogiston Press, 2006.
[35] J. Forest, "New methods for triangulation-based shape acquisition using laser scanners," Ph.D. dissertation, Universitat de Girona, Catalonia, Spain, 2004.
[36] J.-Y. Bouguet and P. Perona, "3D photography on your desk," in *Proc. ICCV*, 1998, pp. 43–50.
[37] C. Matabosch, J. Salvi, D. Fofi, and F. Meriaudeau, "A refined range image registration technique for multi-stripe laser scanner," *Proc. SPIE—Mach. Vis. Appl.*, pp. 1–8, 2006.
[38] R. Hartley and A. Zisserman, *Multiple View Geometry in Computer Vision*. Cambridge, U.K.: Cambridge Univ. Press, 2000.
[39] G. Eren, O. Aubreton, F. Meriaudeau, L. A. Sanchez Secades, D. Fofi, F. Truchetet, and A. Erçil, "Scanning from heating: 3D shape estimation of transparent objects from local surface heating," *Opt. Express*, vol. 17, no. 14, pp. 11 457–11 468, Jul. 2009.
[40] O. Faugeras and Q.-T. Luong, *The Geometry of Multiple Images*. Cambridge, MA: MIT Press, 2001.
[41] M. B. Hullin, M. Fuchs, I. Ihrke, H.-P. Seidel, and H. P. A. Lensch, "Fluorescent immersion range scanning," *ACM Trans. Graphics*, vol. 27, no. 3, pp. 87:1–87:10, Aug. 2008.
[42] N. J. W. Morris and K. N. Kutulakos, "Reconstructing the surface of inhomogeneous transparent scenes by scatter-trace photography," in *Proc. IEEE 11th ICCV*, 2007, pp. 1–8.

Fabrice Mériaudeau was born in Villeurbanne, France, on March 18, 1971. He received the M.S. degree in physics, the engineering degree (FIRST) in material sciences in 1994, and the Ph.D. degree in image processing in 1997 from Dijon University, Dijon, France.

He was a Postdoctoral Researcher for one year with The Oak Ridge National Laboratory, Oak Ridge, TN. He is currently a "Professeur des Universités," the Head of the "University Center Condorcet," and the Deputy Director of the Le2i, Unite Mixte de Recherche, Centre National de la Recherche Scientifique 5158, University de Bourgogne, Le Creusot, France. He is also currently the coordinator of an Erasmus Mundus Master in the field of computer vision and robotics. He has authored or coauthored more than 150 international publications. He is the holder of three patents. His research interests are focused on image processing for artificial vision inspection, particularly on nonconventional imaging systems (UV, IR, polarization, etc.).

Dr. Mériaudeau was the Chairman of The International Society for Optical Engineers' Conference on Machine Vision Application on industrial inspection. He is also a member of numerous technical committees of international conferences in the area of computer vision.

L. Alonso Sánchez Secades received the B.S. degree in electronics engineering from the Institute Tecnológico de Costa Rica, Cartago, Costa Rica, and the M.Sc. degree from the Université de Bourgogne, Dijon, France, Heriot-Watt University, Edinburgh, U.K., and Universitat de Girona, Catalonia, Spain. He is currently working toward the Ph.D. degree in the Laboratoire d'Informatique, de Robotique et de Microélectronique de Montpellier, Centre National de la Recherche Scientifique 5158, University de Bourgogne, Le Creusot, France.

His research activities include medical robotics, 3-D vision, robotic control, and design theory. He has also several industrial experiences, mainly as a research and development engineer.

Gonen Eren received the B.S. and M.S. degrees in computer engineering from Galatasaray University, Istanbul, Turkey, in 2004 and 2007, respectively. He is currently working toward the Ph.D. degree at Sabanci University, Istanbul, and the University of Burgundy, Dijon, France.

A. Erçil was born in Turkey in 1958. She received the B.S. degrees in electrical engineering and in mathematics from Boğaziçi University, Istanbul, Turkey, in 1979 and the M.S. and Ph.D. degrees in applied math from Brown University, Providence, RI, in 1980 and 1983, respectively.

She is currently with the Faculty of Engineering and Natural Sciences, Sabancı University, Istanbul, where she is the Founding Director of VPALAB, which was selected by the European Union as a "potential center of excellence." She is the Founding President of the Turkish Pattern Analysis and Image Processing Group. Her specific research interests include invariant object recognition, shape modeling, texture analysis, biometrics, and image segmentation.

Prof. Erçil has directed many national and international projects (Nato, FP4, Eureka, NSF, FP6, Nedo) and is the Founding Partner and Chief Execute Officer of a spin-off company Vistek A.Ş.

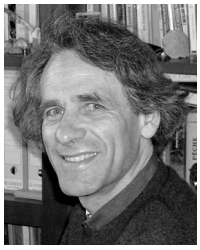

Fred Truchetet was born in Dijon, France, on October 13, 1951. He received the M.S. degree in physics and the Ph.D. degree in electronics from Dijon University, Dijon, in 1973 and 1977, respectively.

For two years, he was with Thomson-CSF as a Research Engineer. He is currently a "Professeur des Universités" with Le2i, Unite Mixte de Recherche, Centre National de la Recherche Scientifique 5158, University de Bourgogne, Le Creusot, France, where he is also the Vice President. He has authored or coauthored more than 150 international publications and three books. He is the holder of three patents. His research interests are focused on image processing for artificial vision inspection, particularly on wavelet transform, edge detection, and 3-D image processing.

Dr. Truchetet is a member of the Groupe de Recherche et d'Etudes du Traitement du Signal et des Images and The International Society for Optical Engineers (SPIE). He was the Chairman of the SPIE Conference on wavelet applications in industrial processing and a member of numerous technical committees of international conferences in the area of computer vision.

Olivier Aubreton was born in Vichy on August 31, 1973. He received the aggregation examination in 2000 and the D.E.A. degree (equivalent to the M.S. degree) in image processing in 2001.

Since September 2005, he has been an Assistant Professor with the Laboratory Le2i (Vision 3-D team), Institut Universitaire de Technologie, Le Creusot, France. His research interests include the design, development implementation, and testing of silicon retinas for pattern matching and pattern recognition. He is currently working on two subjects: the development of new solutions for 3-D reconstruction of problematic surfaces (specular and transparent objects) and the development of 3-D processing approaches for salient point detection on 3-D meshes.

David Fofi received the Ph.D. degree in robotics and computer vision from the University of Picardie Jules Verne, Amiens, France, in 2001.

Since September 2002, he has been a Researcher with the Laboratory Le2i, Unite Mixte de Recherche, Centre National de la Recherche Scientifique 5158, University de Bourgogne, Le Creusot, France, where, in 2007, he became the Head of the 3-D Vision Team. He is currently a Full Professor with the University of Burgundy, Dijon, France. His main research interests include 3-D vision, projector-camera systems, structured light, and catadioptric vision.